Chapter 4

Results and Discussion

In this chapter represents 7 topics viz, results of thermoelectric materials synthesis, crystal structure analysis, microstructure analysis, thermoelectric properties, thermoelectric devices fabrication, possibility to thermoelectric generator and refrigerator and references.

Thermoelectric Materials Synthesis

$Mn_{1-x}Ag_xSi_{1.75-y}Bi_y$ (x = y = 0, 0.01, 0.02, 0.03, 0.04 and 0.05)

The result of $Mn_{1-x}Ag_xSi_{1.75-y}Bi_y$ (x = y = 0, 0.01, 0.02, 0.03, 0.04 and 0.05) materials synthesis are show in Figure 17. Starting materials Mn, Si, Ag and Bi powder exhibit brown, black, write and silver color, respectively. Mixed powders after bill milling was observed homogeneous color. The hot press method was obtained pellet dimeter size of 10 mm and 20 mm of height. The hot press pellet was cut in size of 3×3×15 mm^3 for bulk density and thermoelectric properties measurement, 10×10×1 mm^3 for XRD, hall coefficient and SEM analysis, 2×2×3 mm^3 for thermoelec devices fabrication.

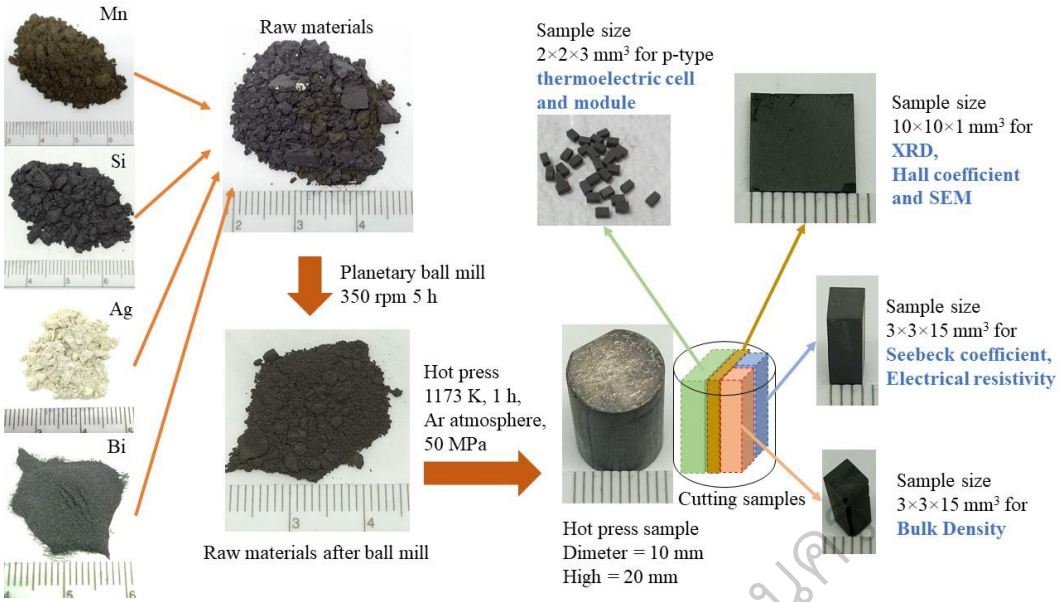

Figure 17 The step detail of $Mn_{1-x}Ag_xSi_{1.75-y}Bi_y$ material synthesis

$Mg_{2-x}Ag_xSi_{1-y}Bi_y$ (x = y = 0, 0.01, 0.02, 0.03, 0.04 and 0.05)

The result of $Mg_{2-x}Ag_xSi_{1-y}Bi_y$ (x = y = 0, 0.01, 0.02, 0.03, 0.04 and 0.05) materials synthesis are show in Figure 18. Starting materials Mg, Si, Ag and Bi powder exhibit silver, black, write and silver color, respectively. Mixed powders after bill milling was observed homogeneous color. The hot press method was obtained pellet dimeter size of 10 mm and 20 mm of height. The hot press pellet was cut in size of 3×3×15 mm^3 for bulk density and thermoelectric properties measurement, 10×10×1 mm^3 for XRD, hall coefficient and SEM analysis, 2×2×3 mm^3 for thermoelec devices fabrication.

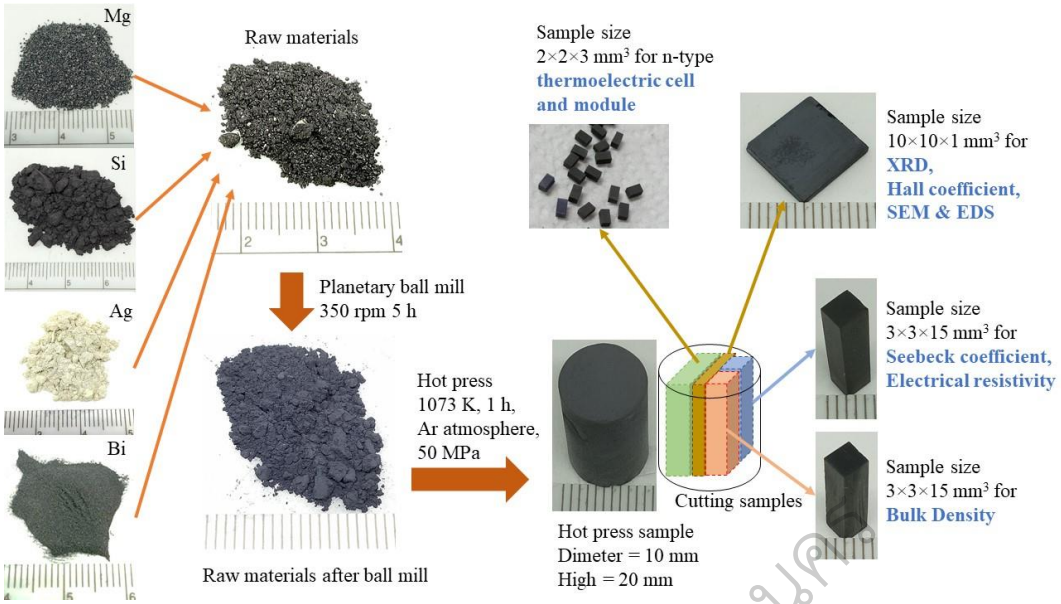

Figure 18 The step detail of $Mg_{2-x}Ag_xSi_{1-y}Bi_y$ materials synthesis

Crystal Structure

$Mn_{1-x}Ag_xSi_{1.75-y}Bi_y$ (x = y = 0, 0.01, 0.02, 0.03, 0.04 and 0.05)

The crystal structure of $Mn_{1-x}Ag_xSi_{1.75-y}Bi_y$ (x = y = 0, 0.01, 0.02, 0.03, 0.04 and 0.05) bulk samples was analyzed by X-ray diffraction technique in scan rang 20-80 degree of 2θ for 2 deg/min of scan speed with 0.02 of sampling pitch. The XRD pattern of all samples show mixes phase between $MnSi_{1.75}$ for main phase and MnSi for secondary phase as shown in Figure 19. This mixes phase was also observed in the samples containing a large amount of MnSi prepared by mechanical alloying followed by hot-pressing or SPS (Chen, X., Shi, L., Zhou, J., & Goodenough, J. B. 2015, pp. 30–36; Shin, D. K., Jang, K. W., Ur, S. C., & Kim, I. H. , 2013, 1756-1761; Lee, Y. G., Choi, M. K., Kim, I. H., & Ur, S. C., 2012, pp, 816-819; Itoh, T., & Yamada, M., 2009, 925). The main phase is shows tetragonal structure with P-4n2 (118) of space group. The calculated lattice parameters are good agreement with ICDD data file no. 00-026-1251 (a = b = 5.53 Å and c = 117.9 Å), however x value affect to slightly increased lattice parameter of a and b while c decreases until x = y = 0.04 as shown in Figure 20 (a). The calculated volume of

unit cell ($V_C = a^2c\ \text{mm}^3$) decreased with increasing x values as shown in Figure 20 (b). Bulk samples were calculated crystal size by Scherrer equation (d =λ/β_s cosθ; where d is crystal size, λ is wave length of X-ray and β_s is Full width at half maximum) that show trend increasing with x value as shown in Figure 20 (c). The theoretical density was calculated by $T.D. = nA/V_C N_A$ (where n is number of atoms in unit cell, A is atomic weight, V_C is volume of unit cell and N_A is Avogado's number = 6.023×10^{23} atoms/mol) for compared with bulk density to get the relative density. Figure 20 (d) shows the relative density of all samples higher than 92% indicating that the hot press method was successfully to prepare high density samples.

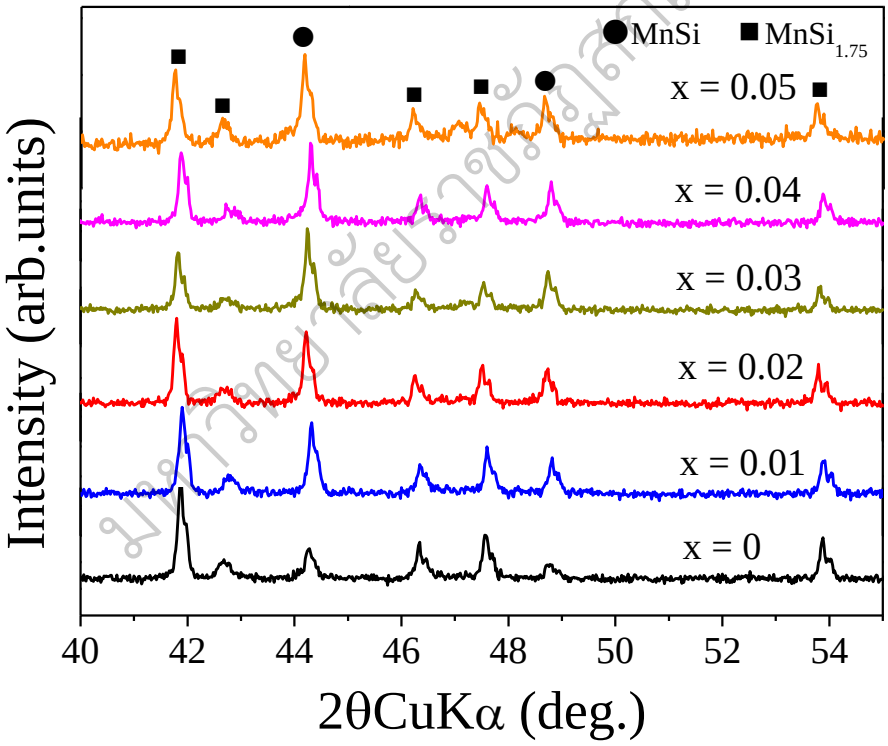

Figure 19 XRD patterns of $Mn_{1-x}Ag_xSi_{1.75-y}Bi_y$ bulks

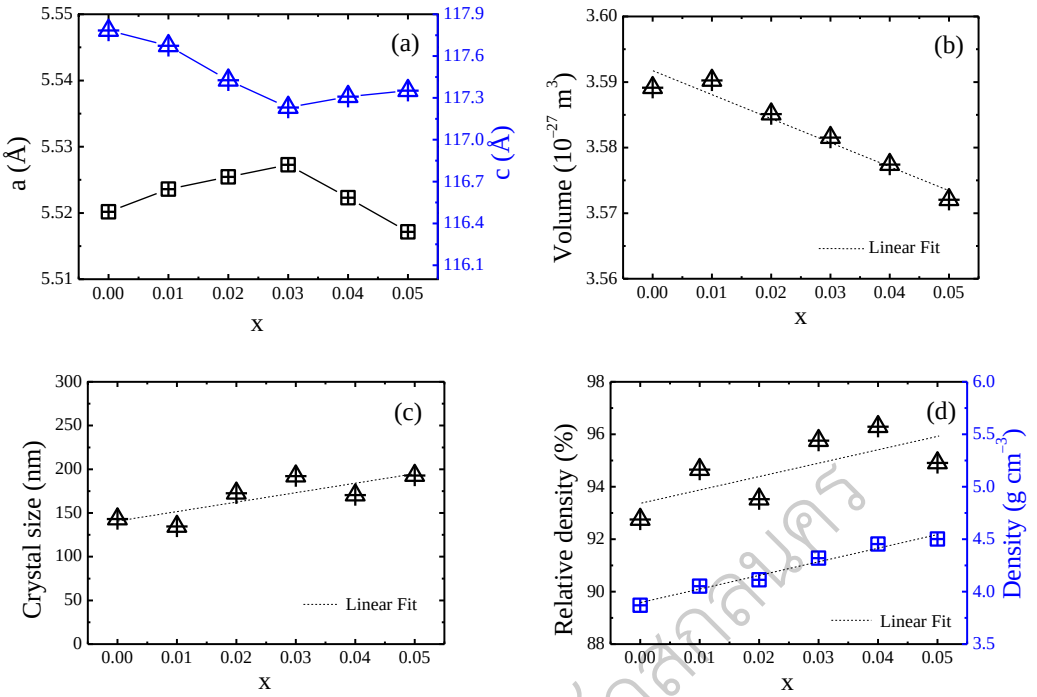

Figure 20 (a) Lattice parameter, (b) Volume of unit cell, (c), Crystal size, (d) Relative density and bulk density as a function of x values of $Mn_{1-x}Ag_xSi_{1.75-y}Bi_y$ bulk samples

$Mg_{2-x}Ag_xSi_{1-y}Bi_y$ (x = y = 0, 0.01, 0.02, 0.03, 0.04 and 0.05)

The crystal structure of $Mg_{2-x}Ag_xSi_{1-y}Bi_y$ (x = y = 0, 0.01, 0.02, 0.03, 0.04 and 0.05) bulk samples was analyzed by X-ray diffraction technique in scan rang 20-80 degree of 2θ for 2 deg/min of scan speed with 0.02 of sampling pitch as shown in Figure 21. The XRD pattern of all samples show cubic structure and corresponded with PDF Card number 00-035-0773. However, MgO peak was observed effect from oxidation reaction. The MgO phase was also observed in the samples prepared by mechanical alloying followed by hot-pressing (Kim, G., Lee, H., Kim, J., Roh, J. W., Lyo, I., Kim, B. W., ... & Lee, W., 2017, 53-56; Kim, et al., 2016, pp. 11-15; Delgado, A., Cordova, S., Lopez, I., Nemir, D., & Shafirovich, E., 2016, pp. 422-429; Satyala, N., Krasinski, J. S., & Vashaee, D. 2014, pp. 141-150). The presence of small amount of MgO phase (weak peak at 2θ = 43°); a common impurity for this type of material (Vlachos, N., et al., 2017, pp. 502-513). The Ag

peak was observed only $Mg_{2-x}Ag_xSi_{1-y}Bi_y$ effecting to good conductive. The calculated lattice parameters are good agreement with ICDD data file no. 00-035-0773 (a = b = c = 6.35119 Å), however x value affect to slightly decreased lattice parameter until x = y = 0.04 after that lattice parameter was decreased as shown in Figure 22 (a). The calculated volume of unit cell ($V_C = a^2\ \mathrm{mm}^3$) decreased with inceasing x values until x = y = 0.04 after that increases as shown in Figure 22 (b). Bulk samples were calculated crystal size that show trend increasing with x value as shown in Figure 22 (c). Bulk density of $Mg_{2-x}Ag_xSi_{1-y}Bi_y$ samples were increasing with increasing x values while relative density decreased as shown in Figure 22 (d).

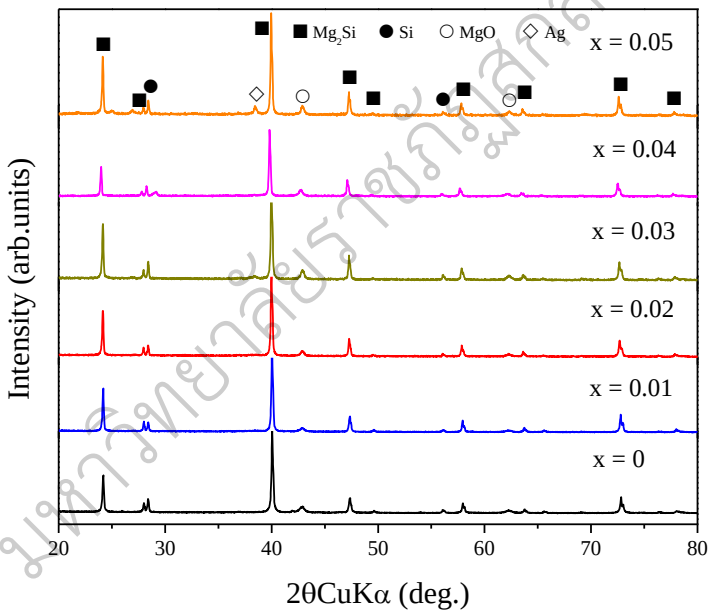

Figure 21 XRD patterns of $Mg_{2-x}Ag_xSi_{1-y}Bi_y$ bulk samples

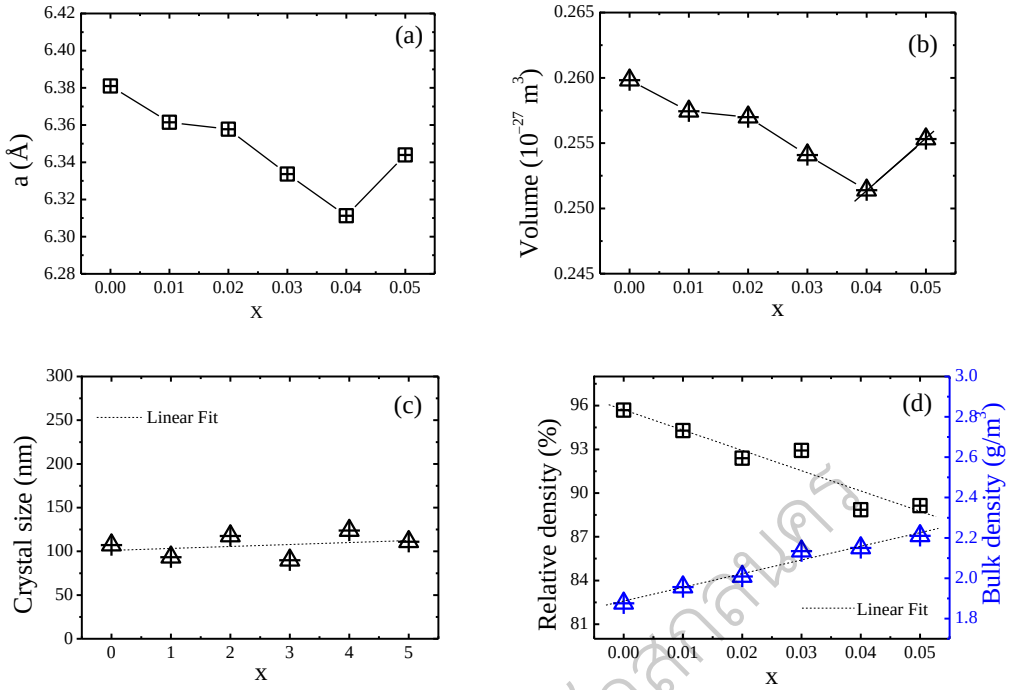

Figure 22 (a) Lattice parameter, (b) Crystal size, (c) Volume of unit cell, (d) Relative density and bulk density as a function of x values of $Mg_{2-x}Ag_xSi_{1-y}Bi_y$ bulk samples

Microsructure Analysis

$Mn_{1-x}Ag_xSi_{1.75-y}Bi_y$ (x = y = 0, 0.01, 0.02, 0.03, 0.04 and 0.05)

SEM micrograph of $Mn_{1-x}Ag_xSi_{1.75-y}Bi_y$ (x = y = 0, 0.01, 0.02, 0.03, 0.04 and 0.05) bulk samples show in Figure 23 (a)-(f). The Ag and Bi doped can be inserted in the vacancy between the grain of materials cause to get high density of the sample. The elemental mapping of $Mn_{1-x}Ag_xSi_{1.75-y}Bi_y$ bulk samples were obtained by Oxford Instruments detector. The elemental mapping of all samples shows homogenous distribution of Mn, Si, Ag and Bi that confirmed completely mixing by planetary ball mill method as shown in Figure 24 (a)-(f). The energy dispersive X-ray spectroscopy (EDS) was analyzed, and show the results agree with the composition of initial atomic ratio, however Bi element can't observe in x = y = 0.01 condition as shown in table 5.

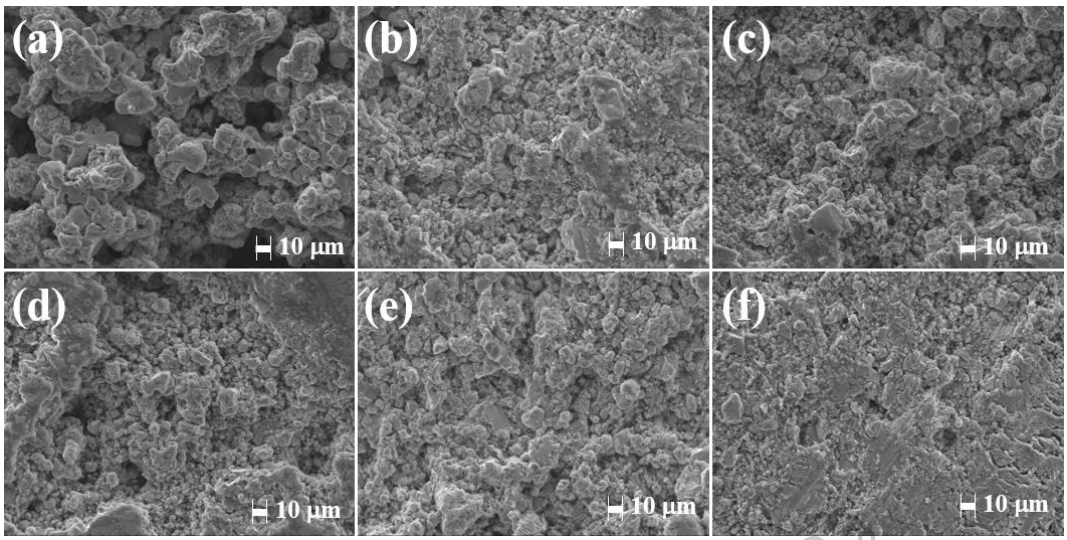

Figure 23 SEM micrographs of $Mn_{1-x}Ag_xSi_{1.75-y}Bi_y$ bulk samples (a) x = y = 0, (b) x = y = 0.01, (c) x = y = 0.02, (d) x = y = 0.03 and (e) x = y = 0.04 and (f) x = y = 0.05

Table 5 The EDS of $Mn_{1-x}Ag_xSi_{1.75-y}Bi_y$ (x = y = 0, 0.01, 0.02, 0.03, 0.04 and 0.05) bulk samples

Materials	Si (At%)	Mn (At%)	Ag (At%)	Bi (At%)
$MnSi_{1.75}$	61.18	38.82		
$Mn_{0.99}Ag_{0.01}Si_{1.74}Bi_{0.01}$	61.93	37.35	0.72	
$Mn_{0.98}Ag_{0.02}Si_{1.73}Bi_{0.02}$	63.54	34.58	0.94	0.94
$Mn_{0.97}Ag_{0.03}Si_{1.72}Bi_{0.03}$	43.06	55.22	0.92	0.8
$Mn_{0.96}Ag_{0.04}Si_{1.71}Bi_{0.04}$	57.87	39.95	1.09	1.09
$Mn_{0.95}Ag_{0.05}Si_{1.70}Bi_{0.05}$	59.17	36.49	2.17	2.17

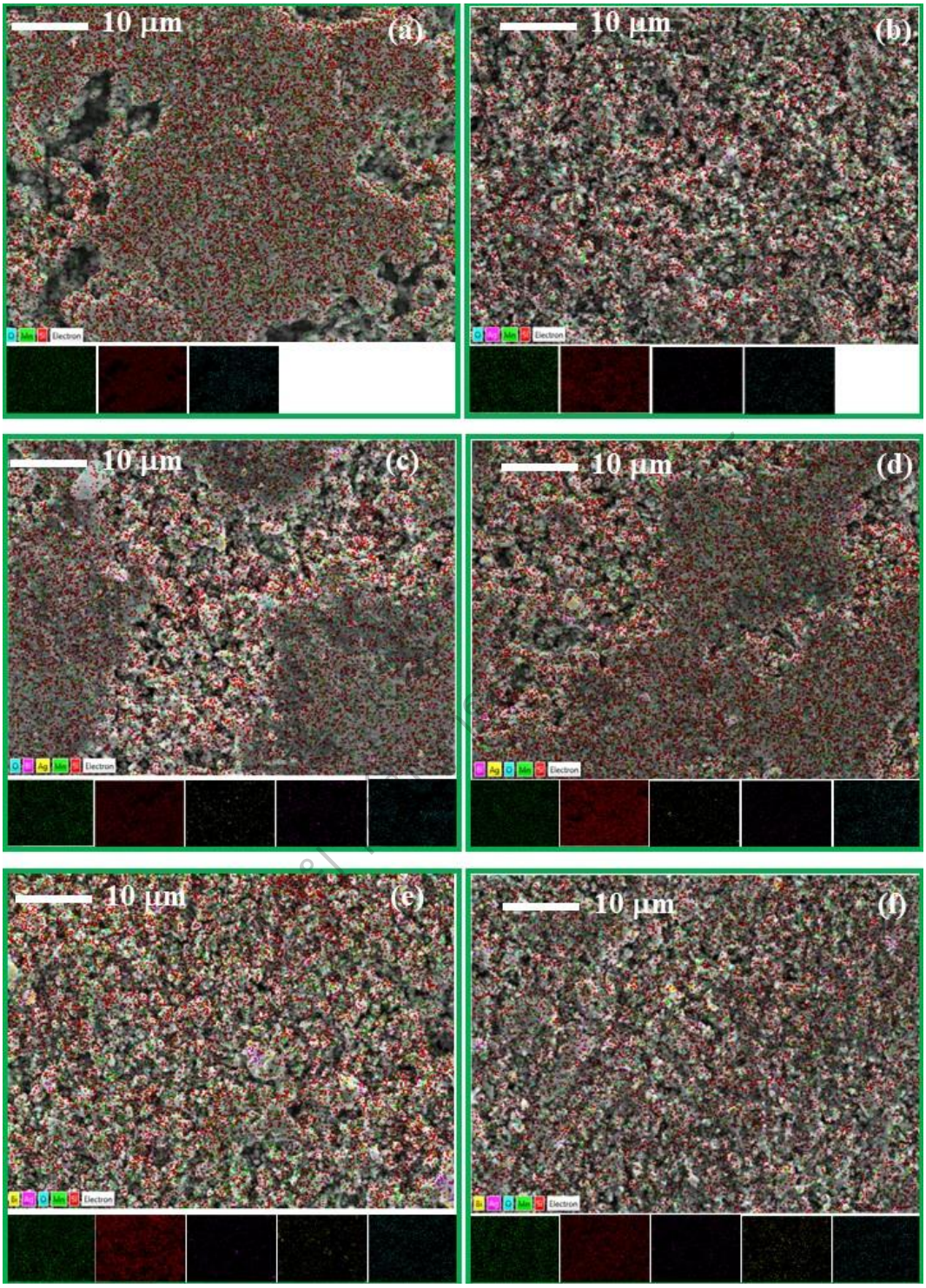

Figure 24 Elemental mapping of $Mn_{0.96}Ag_{0.04}Si_{1.71}Bi_{0.04}$ surface bulk samples (a) x = y = 0, (b) x = y = 0.01, (c) x = y = 0.02, (d) x = y = 0.03 and (e) x = y = 0.04 and (f) x = y = 0.05

$Mg_{2-x}Ag_xSi_{1-y}Bi_y$ (x = y = 0, 0.01, 0.02, 0.03, 0.04 and 0.05)

SEM micrograph of $Mg_{2-x}Ag_xSi_{1-y}Bi_y$ (x = y = 0, 0.01, 0.02, 0.03, 0.04 and 0.05) bulk samples show in Figure 25 (a)-(f). These samples are closely packed, consistent with the high density of bulk samples and the grain size of the sample is almost in the micron-scale range. In addition, there are much smaller particles, which is believed to be able to lower the thermal conductivity by scattering the heat-carrying phonons covering the broad phonon free paths (Tang, X., et al., 2017, pp.1396-1400). The elemental mapping of $Mg_{2-x}Ag_xSi_{1-y}Bi_y$ bulk samples shows homogenous distribution of Mg, Si, Ag and Bi that confirmed completely mixing by planetary ball mill method as shown in Figure 26 (a)-(f). However, Si element spots (green colour) of all samples were found. The energy dispersive X-ray spectroscopy (EDS) the results agree with the composition of initial atomic ratio as shown in table 6.

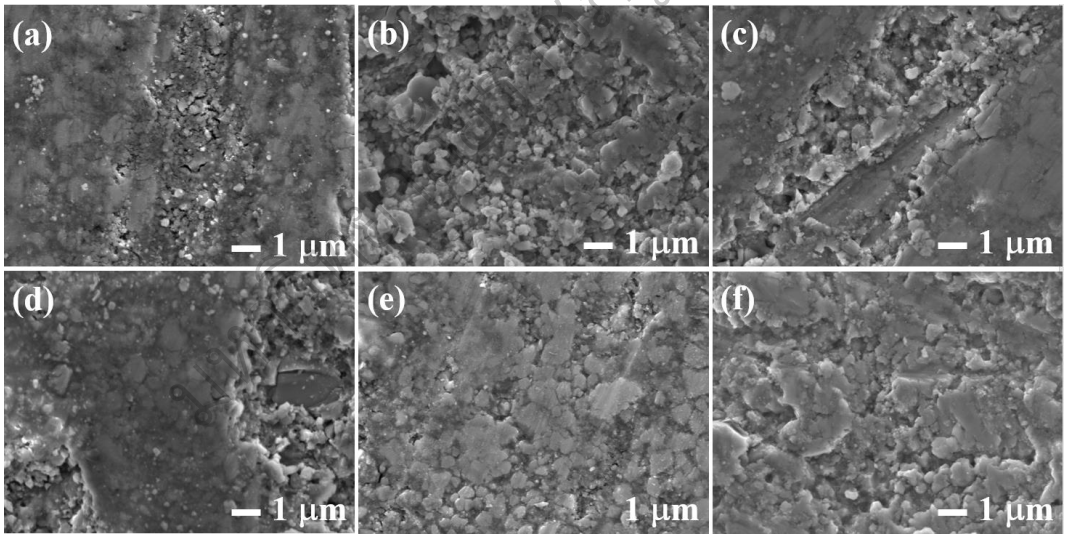

Figure 25 SEM micrographs of $Mg_{2-x}Ag_xSi_{1-y}Bi_y$ bulk samples (a) x = y = 0, (b) x = y = 0.01, (c) x = y = 0.02, (d) x = y = 0.03 and (e) x = y = 0.04 and (f) x = y = 0.05

Table 6 The EDS of $Mg_{2-x}Ag_xSi_{1-y}Bi_y$ (x = y = 0, 0.01, 0.02, 0.03, 0.04 and 0.05) bulk samples

Bulk samples	Si (At%)	Mg (At%)	Ag (At%)	Bi (At%)
x = y = 0.00	30.65	69.35	0	0
x = y = 0.01	29.25	70.13	0.31	0.31
x = y = 0.02	28.7	69.73	0.64	0.93
x = y = 0.03	29.24	70.12	0.32	0.32
x = y = 0.04	32.2	66.15	0.75	0.9
x = y = 0.05	30.1	67.1	1.17	1.63

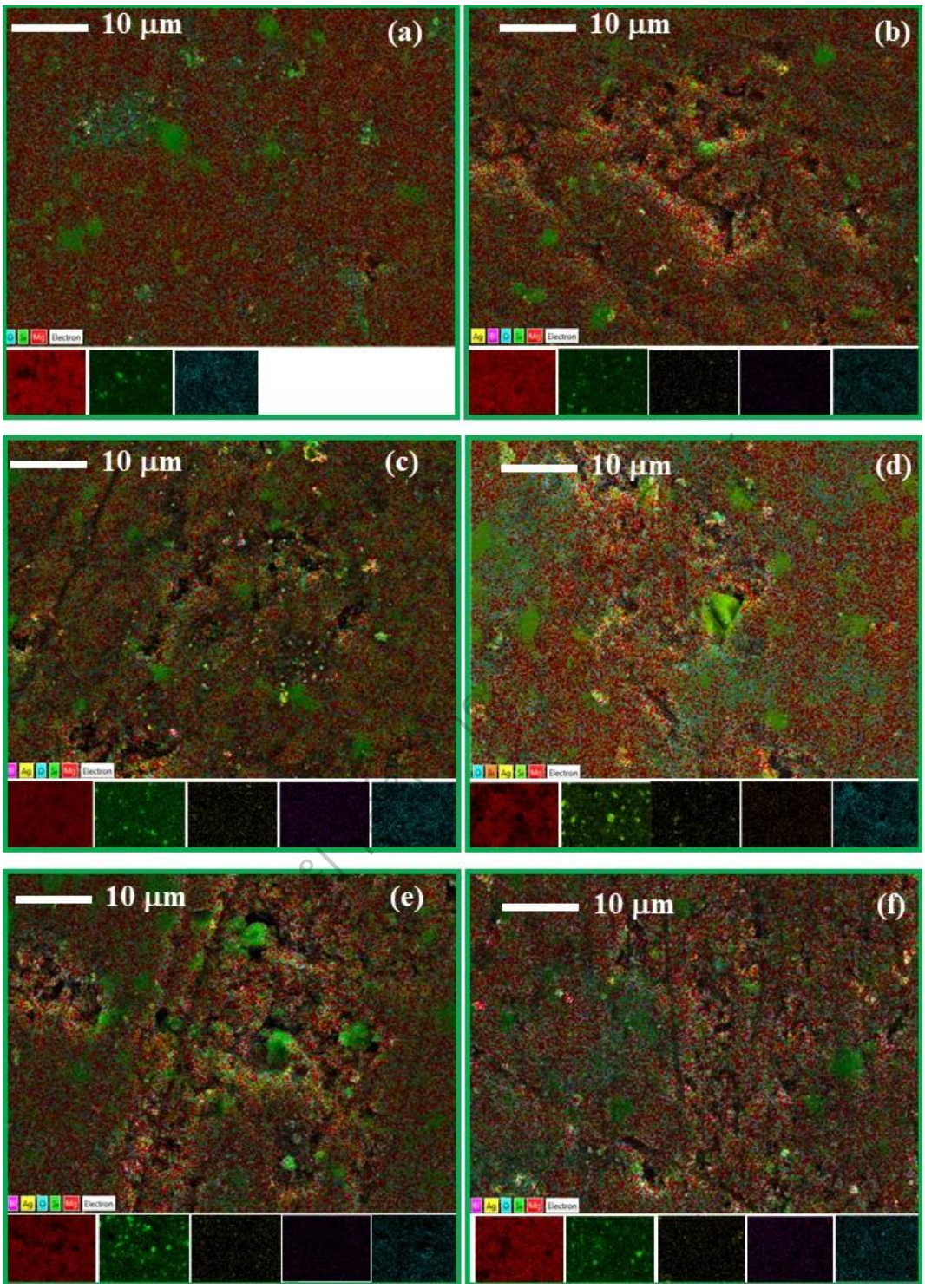

Figure 26 Elemental mapping of $Mg_{2-x}Ag_xSi_{1-y}Bi_y$ surface bulk samples (a) x = y = 0, (b) x = y = 0.01, (c) x = y = 0.02, (d) x = y = 0.03 and (e) x = y = 0.04 and (f) x = y = 0.05

Thermoelectric Properties

$Mn_{1-x}Ag_xSi_{1.75-y}Bi_y$ (x = y = 0, 0.01, 0.02, 0.03, 0.04 and 0.05)

1. Seebeck coefficient

The Seebeck coefficient of $Mn_{1-x}Ag_xSi_{1.75-y}Bi_y$ (x = y = 0, 0.01, 0.02, 0.03, 0.04 and 0.05) bulk samples in temperature ranges 300-773 K comparing with literlature data (Sadia, Y., Dinnerman, L., & Gelbstein, Y., 2013, pp. 1926-1931) are show in Figure 27. All the samples are observed Seebeck coefficient in positive value which means the samples have p-type conduction and that most of the carriers are holes (Shin, D. K., Ur, S. C., Jang, K. W., & Kim, I. H., 2014, pp. 2104-2108). The Seebeck coefficient aspect linear increase up to the maximum at 650 – 700 K and then decreases. The Seebeck coefficient of doped samples are show all higher than undoped sample. The highest of S value reveal by $Mn_{0.98}Ag_{0.02}Si_{1.73}Bi_{0.02}$ sample about 119 μV K^{-1} at 673 K. The key parameters of Seebeck coefficient for semiconductors behavior as follow by Eq. 4.1 (Snyder, G. J., & Toberer, E. S., 2011, pp. 101-110).

$$S = \frac{8\pi^2 k_B^2}{3eh^2} \mathrm{m}^* \left(\frac{\pi}{3n}\right)^{2/3} T, \qquad (4.1)$$

where k_B is Boltzmann's constant, e is the electronic charge, h is Planck's constant, m^* is the effective mass and n is the carrier concentration. The carrier concentration and mobility were obtained from hall effect measurement system as shown in table 7. The carrier concentration of undoped $MnSi_{1.75}$ is 1.3×10^{17} cm^{-3}, which was increased to 1.61×10^{17} - 2.82×10^{17} cm^{-3} by Ag and Bi doped.

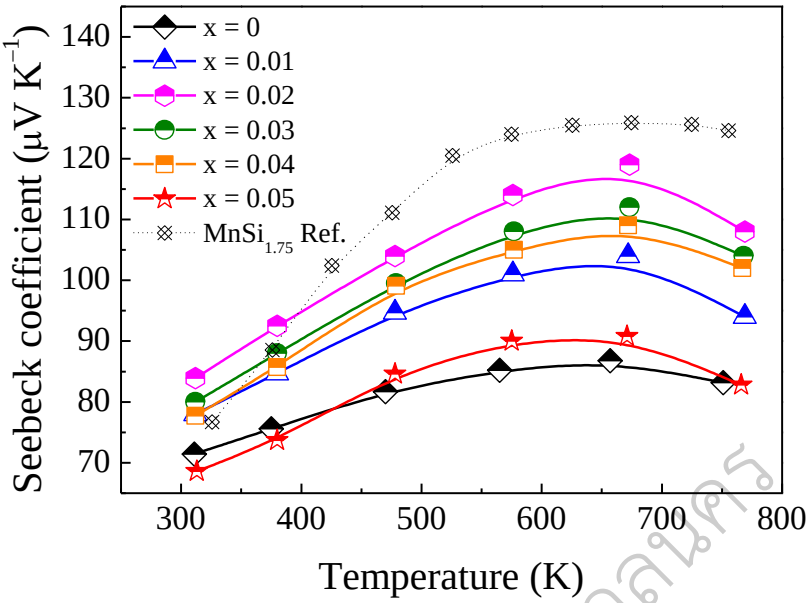

Figure 27 Seebeck coefficient dependence on temperature of $Mn_{1-x}Ag_xSi_{1.75-y}Bi_y$ bulk samples (Sadia, Y., Dinnerman, L., & Gelbstein, Y., 2013, pp. 1926-1931)

Table 7 Transport properties of $Mn_{1-x}Ag_xSi_{1.75-y}Bi_y$ at 300 K

Bulk samples	Mobility ($cm^2 V^{-1}s^{-1}$)	Carrier concentration (cm^{-3})	Resistivity (mΩ cm)
x = y = 0.00	2.32×10^3	1.30×10^{17}	0.75
x = y = 0.01	9.72×10^2	1.82×10^{17}	0.53
x = y = 0.02	9.52×10^2	1.81×10^{17}	0.58
x = y = 0.03	2.05×10^3	1.61×10^{17}	0.53
x = y = 0.04	3.30×10^3	2.27×10^{17}	0.34
x = y = 0.05	2.41×10^3	2.82×10^{17}	0.20

2. Electrical resistivity

The electrical resistivity of $Mn_{1-x}Ag_xSi_{1.75-y}Bi_y$ (x = y = 0, 0.01, 0.02, 0.03, 0.04 and 0.05) bulk samples in temperature ranges 300-773 K comparing with literlature data (Barczak, S. A., Downie, R. A., Popuri, S. R., Decourt, R., Pollet,

M., & Bos, J. W. G., 2015, pp. 55-59.) are show in Figure 28. The electrical resistivity shows the order around 10^{-5} Ω m which corresponding with the result form hall effect measurement system as shown in table 7. The doped samples exhibit behaving metallic characteristics in temperature ranges 300-673 K namely the value increased with temperature. After 673 K, the electrical resistivity of doped samples release semi-conductor behavior namely the value decreased when increasing temperature (Zheng, L., et al., 2016, pp. 452-457). The doped samples with x value effect to insignificant increase electrical resistivity. However, all samples show lower than literature data. The electrical resistivity can be defined by Eq. (4.2) and Eq. (4.3) (Godlewska, E. M., Mars, K., Drozdz, P., Tchorz, A., & Ksiazek, M., 2016, pp. 755-764)

$$\rho = \frac{1}{\sigma} = \frac{1}{ne\mu} \tag{4.2}$$

where μ is the carrier mobility, n is the carrier concentration, e is the electron charge and σ is electrical conductivity.

$$\sigma = \frac{A}{T}\exp\left(\frac{-E_a}{k_B T}\right) \tag{4.3}$$

where A is the pre-exponential factor, k_B is Boltzmann's constant (1.38×10^{-23} J/K), T the absolute temperature and E_a the activation energy of conduction.

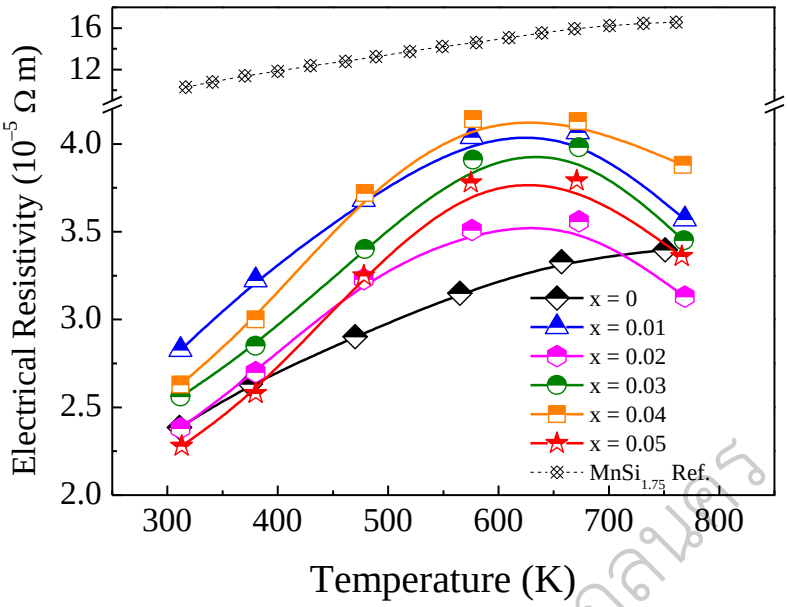

Figure 28 Electrical resistivity dependence on temperature of $Mn_{1-x}Ag_xSi_{1.75-y}Bi_y$ bulk samples (Barczak, S. A., Downie, R. A., Popuri, S. R., Decourt, R., Pollet, M., & Bos, J. W. G., 2015, pp. 55-59)

3. Power factor

The power factor of $Mn_{1-x}Ag_xSi_{1.75-y}Bi_y$ (x = y = 0, 0.01, 0.02, 0.03, 0.04 and 0.05) bulk samples was calculated by Seebeck coefficient and electrical resistivity following $PF = S^2 / \rho$ and show in Figure 29. The power factor of doped samples exhibits higher than non-doped sample except the $Mn_{0.95}Ag_{0.05}Si_{1.70}Bi_{0.05}$. The x values doped on $MnSi_{1.75}$ effected to increasing power factor of 0.01 – 0.02 and then decreased, indicating that limited of doping amount of x value. The $Mn_{0.98}Ag_{0.02}Si_{1.73}Bi_{0.02}$ sample reveal highest power factor about 3.97 × 10^{-4} $Wm^{-1}K^{-2}$ at 673 K, which represents a more than 45.35 % enhancement in comparison to the non-doped $MnSi_{1.75}$ sample. Moreover, the power factor of $Mn_{0.98}Ag_{0.02}Si_{1.73}Bi_{0.02}$ sample show higher than $MnSi_{1.75}$ of literature data (Barczak, S. A., Downie, R. A., Popuri, S. R., Decourt, R., Pollet, M., & Bos, J. W. G., 2015, pp. 55-59) because it shows high S and low ρ. The

$Mn_{0.98}Ag_{0.02}Si_{1.73}Bi_{0.02}$ sample is most suitable for p-tpye of thermoelectric fabrication.

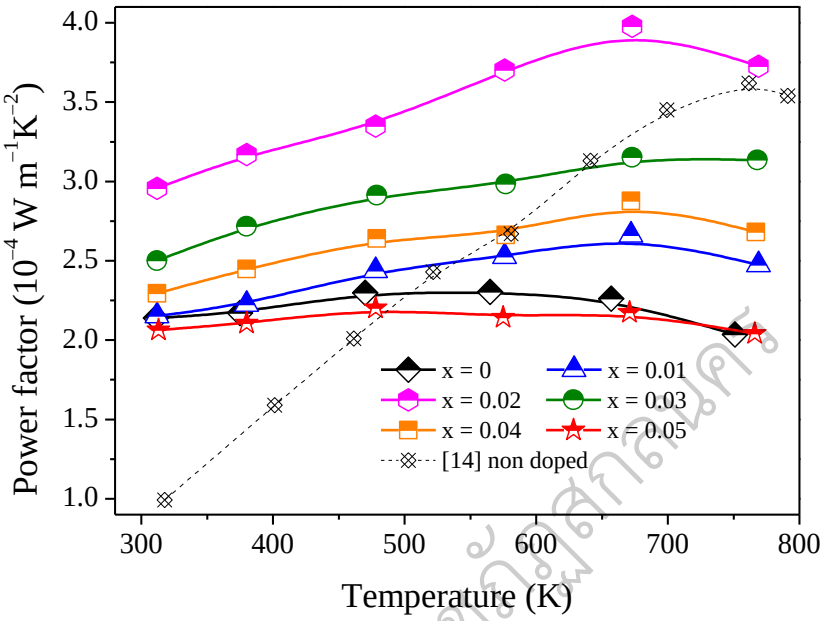

Figure 29 The power factor dependence on temperature of $Mn_{1-x}Ag_xSi_{1.75-y}Bi_y$ bulk samples (Barczak, S. A., Downie, R. A., Popuri, S. R., Decourt, R., Pollet, M., & Bos, J. W. G., 2015, pp. 55-59)

$Mg_{2-x}Ag_xSi_{1-y}Bi_y$ (x = y = 0, 0.01, 0.02, 0.03, 0.04 and 0.05)

1. Seebeck coefficient

The Seebeck coefficient of $Mg_{2-x}Ag_xSi_{1-y}Bi_y$ (x = y = 0, 0.01, 0.02, 0.03, 0.04 and 0.05) bulk samples in temperature ranges 300-773 K comparing with literlature data (Vivekanandhan, P., et al., 2015, pp. 523-531) are show in Figure 30. All the samples are observed Seebeck coefficient in negative value which means the samples have n-type conduction and that most of the carriers are electrons (Tani, J. I., & Kido, H., 2005, pp. 218-224). The Seebeck coefficient of these samples shows decrease when temperature incresing and increased with x value up to 0.02 and then decreased. The Seebeck coefficient of doped samples at 773 K show all higher than undoped sample. The highest of S value reveal by

$Mg_{1.98}Ag_{0.02}Si_{0.98}Bi_{0.02}$ sample about -285.37 μV K^{-1} at 773 K. The carrier concentration and mobility were obtained from hall effect measurement system as shown in table 8. The carrier concentration of undoped Mg_2Si is 1.97×10^{15} cm^{-3}, which was increased to 2.35×10^{15} - 8.05×10^{15} cm^{-3} by Ag and Bi doped.

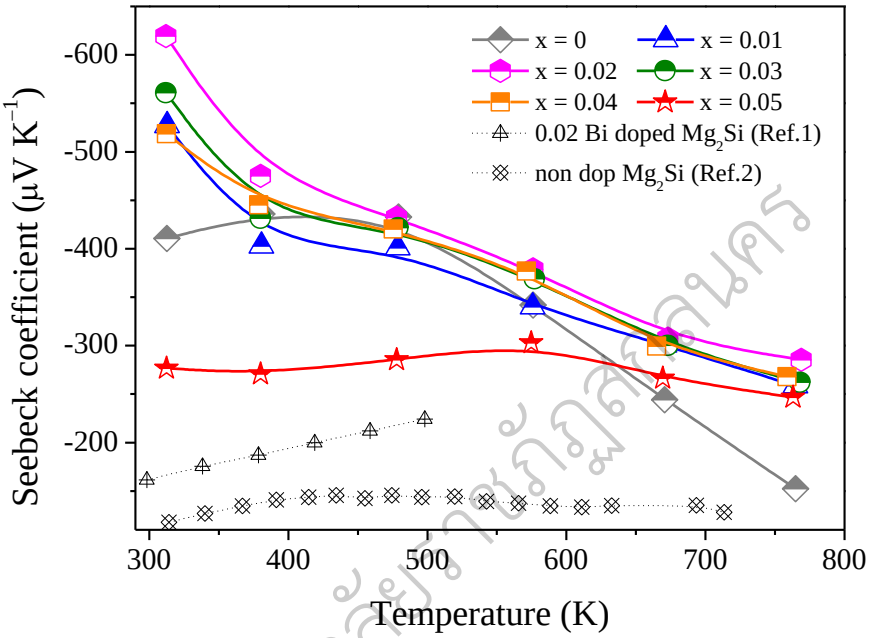

Figure 30 Seebeck coefficient dependence on temperature of $Mg_{2-x}Ag_xSi_{1-y}Bi_y$ bulk samples (Vivekanandhan, P., et al., 2015, pp. 523-531)

Table 8 Transport properties of $Mg_{2-x}Ag_xSi_{1-y}Bi_y$ bulk samples at 300 K

Nominal composition	Mobility (cm^2 $V^{-1}s^{-1}$)	Carrier concentration (cm^{-3})	Resistivity (Ω cm)
x = y = 0.00	1.28×10^3	1.97×10^{15}	241.5
x = y = 0.01	3.39×10^2	2.35×10^{15}	29.25
x = y = 0.02	5.74×10^2	3.43×10^{15}	18.64
x = y = 0.03	3.26×10^3	4.99×10^{15}	37.9
x = y = 0.04	2.63×10^3	8.05×10^{15}	29.7
x = y = 0.05	4.71×10^3	6.72×10^{15}	6.23

2. Electrical resistivity

The electrical resistivity of $Mg_{2-x}Ag_xSi_{1-y}Bi_y$ (x = y = 0, 0.01, 0.02, 0.03, 0.04 and 0.05) bulk samples in temperature ranges 300-773 K comparing with literlature data (Luo, W., Yang, M., Chen, F., Shen, Q., Jiang, H., & Zhang, L., 2009, pp. 96-100; Song, R. B., Aizawa, T., & Sun, J. Q., 2007, pp. 111-117) are show in Figure 31. The electrical resistivity of samples shows the order around 10^{-2} Ω m at room temperature which corresponding with the result form hall effect measurement system. All samples exhibit semi-conductor behavior namely the value decreased when increasing temperature (Zheng, L., et al., 2016, pp. 452-457). The $MnSi_{1.75}$ doded with x values were reduced electrical resistivity indicated that Ag and Bi doped can be increase the carrier concentration as shown in table 4 (Tang, X., et al., 2016, pp. 52-56) The $Mg_{1.95}Ag_{0.05}Si_{0.95}Bi_{0.05}$ bulks sample shows lowest value of electrical resistivity about 3 mΩ cm at 773 K.

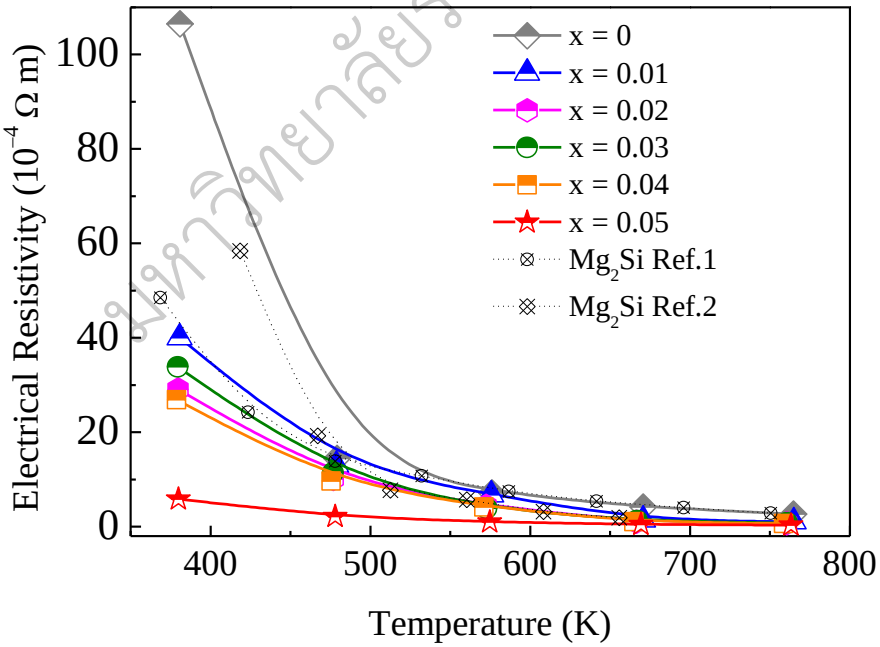

Figure 31 Electrical resistivity dependence on temperature of $Mg_{2-x}Ag_xSi_{1-y}Bi_y$ bulk samples (Luo, W., Yang, M., Chen, F., Shen, Q., Jiang, H., & Zhang, L., 2009, pp. 96-100; Song, R. B., Aizawa, T., & Sun, J. Q., 2007, pp. 111-117)

3. Power factor

The power factor dependence on temperature ranges 300 – 773 K of $Mg_{2-x}Ag_xSi_{1-y}Bi_y$ (x = y = 0, 0.01, 0.02, 0.03, 0.04 and 0.05) bulk samples comparing with literature data (Godlewska, E. M., Mars, K., Drozdz, P., Tchorz, A., & Ksiazek, M., 2016, pp. 755-764) shows in Figure 32. The power factor of doped samples shows increased with increasing temperature corresponding with literature data. The Ag and Bi doped on Mg_2Si effect to enhancing power factor and $Mg_{1.95}Ag_{0.05}Si_{0.95}Bi_{0.05}$ bulks sample shows highest power factor about 20.27 mW cm^{-1} K^{-2}. The $Mg_{1.95}Ag_{0.05}Si_{0.95}Bi_{0.05}$ bulk sample is most suitable for n-tpye of thermoelectric fabrication.

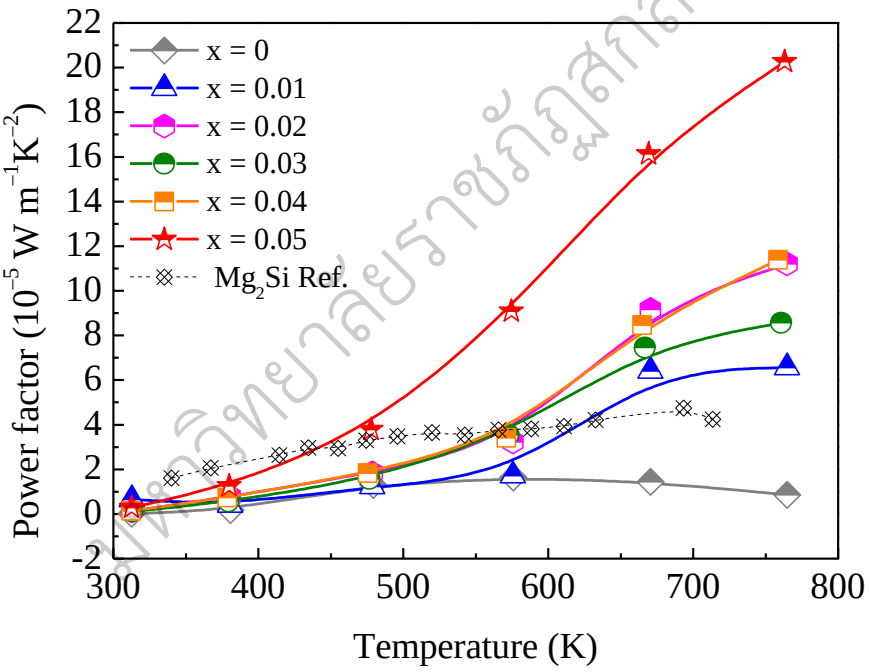

Figure 32 The power factor dependence on temperature of $Mg_{2-x}Ag_xSi_{1-y}Bi_y$ bulk samples (Godlewska, E. M., Mars, K., Drozdz, P., Tchorz, A., & Ksiazek, M. , 2016, pp. 755-764)

Thermoelectric Devices Fabrication

1 pair, 11 pairs and 30 pairs of thermoelectric devices were design by solidworks program as shown in Figure 33 (a), (b) and (c), respectively. The thermoelectric devices were fabricated following the design using $Mn_{0.98}Ag_{0.02}Si_{1.73}Bi_{0.02}$ for p-type and $Mg_{1.95}Ag_{0.05}Si_{0.95}Bi_{0.05}$ for n-type thermoelectric element as shown in Figure 33 (d), (e) and (f). The 1 pair, 11 pairs and 30 pairs of thermoelectric devices exhibit resistance about 2.2 Ω, 21 Ω and 55 Ω, respectively.

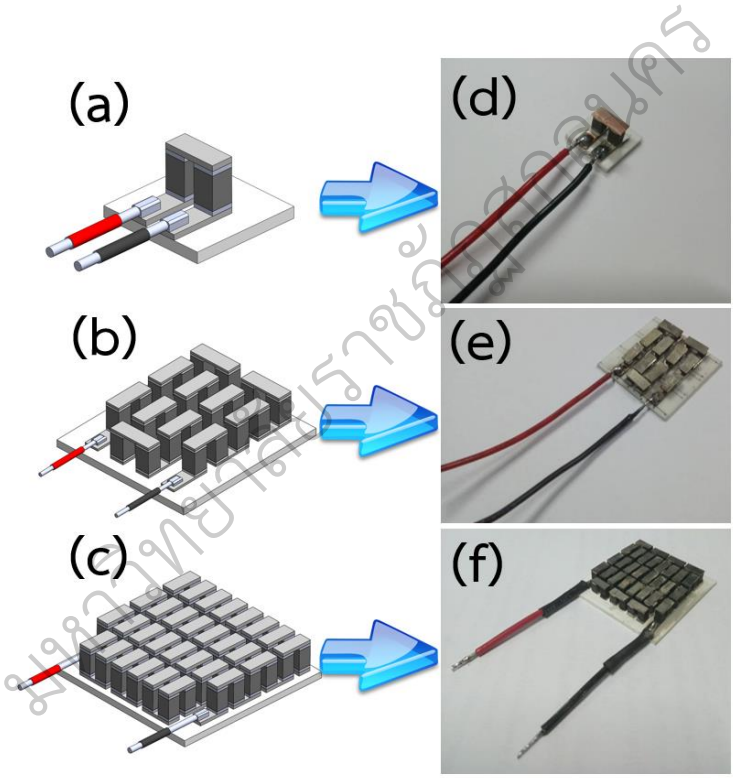

Figure 33 Thermoelectric devices of (a) 1 pair design, (b) 11 pairs design, (c) 30 pairs design, (d) 1 pair fabrication, (e) 11 pairs fabrication and (f) 30 pairs fabrication

Possibility to Thermoelectric Generator and Refrigerator

Thermoelectric generator

1. Electrical voltage of thermoelectric devices

Electrical voltage dependent on different temperature of 1 pair, 11 pairs and 30 pairs of thermoelectric devices are show in Figure 34. All devices show electrical voltage increased with increasing temperature and also increased with the number of pairs indicating the number of pair effect to electrical voltage. The maximum electrical voltage of 1 pair, 11 pairs and 30 pairs of thermoelectric devices are 13.4 mV, 161 mV and 452 mV at different temperature 140 K, respectively.

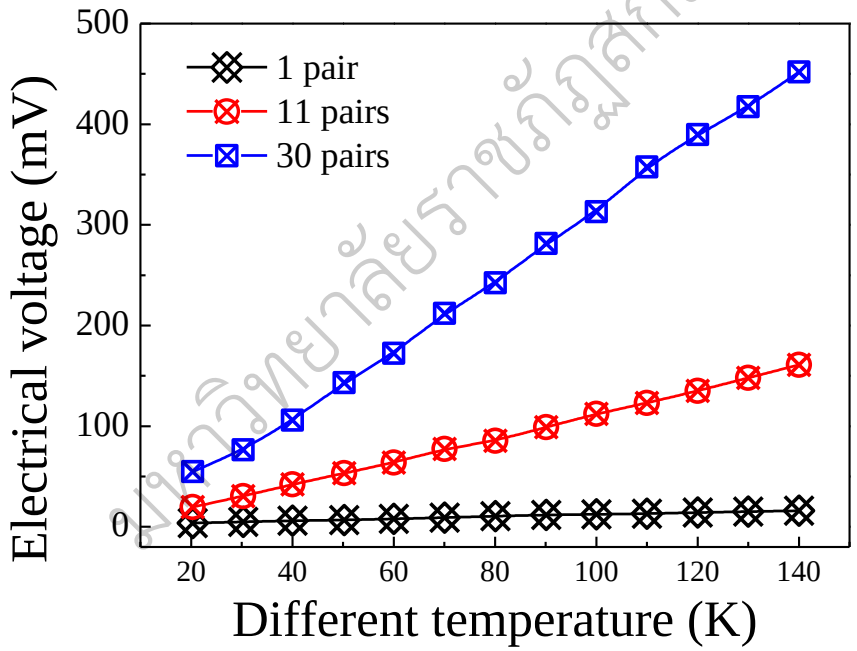

Figure 34 The electrical voltage dependence on different temperature of thermoelectric devices

2. Electrical current of thermoelectric devices

Electrical current dependent on different temperature of 1 pair, 11 pairs and 30 pairs of thermoelectric devices are show in Figure 35. All devices

show electrical current increased with increasing temperature and also increased with the number of pairs indicating the number of pair effect to electrical current. The maximum electrical current of 1 pair, 11 pairs and 30 pairs of thermoelectric devices are 6.7 mA, 8.05 mA and 9.04 mA at different temperature 140 K, respectively.

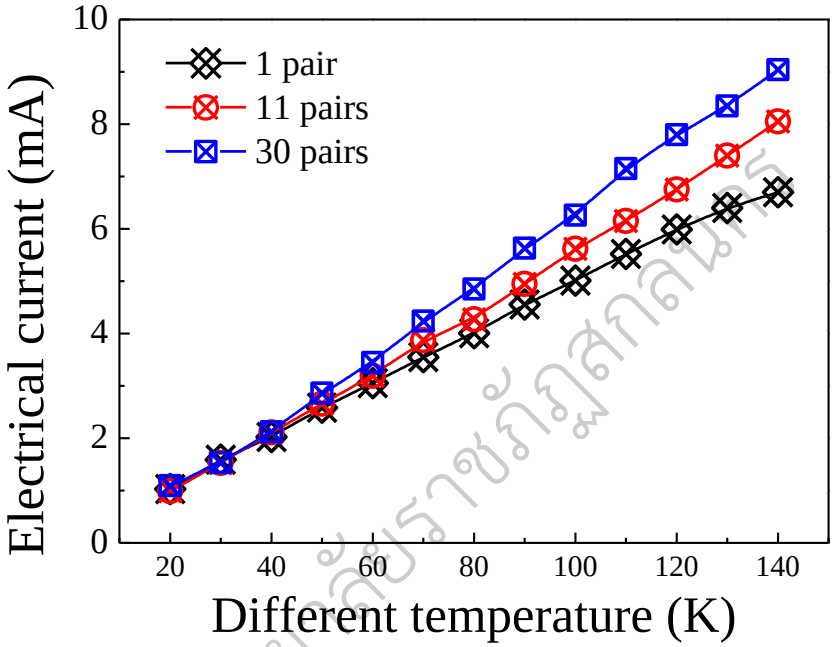

Figure 35 The electrical current dependence on different temperature of thermoelectric devices

3. Electrical power

The electrical power dependence on different temperature of 1 pair, 11 pairs and 30 pairs of thermoelectric devices are show in Figure 36. The measurement power output was used matching load of 2 Ω for 1 pair, 20 Ω for 11 pairs and 50 Ω for 30 pairs. The electrical power of thermoelectric devices increased with increasing temperature. The 1 pair, 11 pairs and 30 pairs of thermoelectric devices show the maximum electrical power about 0.08 mW, 1.29 mW and 4.08 mW at different temperature 140 K, respectively. The electrical power of 11 pairs and 30 pairs show higher than 1 pair about 14.43 and 45.51

times confirm that, the thermoelectric materials and electrode related to good contact.

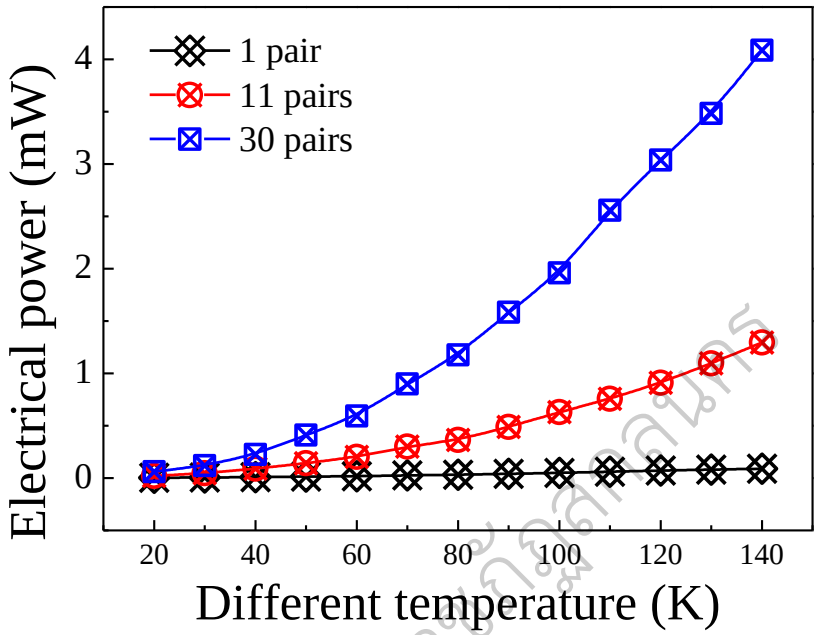

Figure 36 The electrical current dependence on different temperature of thermoelectric devices

Thermoelectric refrigerator

The surface temperature dependence on electrical voltage of 1 pair, 11 pairs and 30 pairs of thermoelectric devices are show in Figure 37. The surface temperature of all devices was slightly decreased when increasing electrical voltage. The 1 pair, 11 pairs and 30 pairs show maximum surface temperature decreased about 0.05 K (10 V), 0.09 K (12 V) and 0.17 K (V), respectively. The thermoelectric devices of p-$Mn_{0.98}Ag_{0.02}Si_{1.73}Bi_{0.02}$ and n-$Mg_{1.95}Ag_{0.05}Si_{0.95}Bi_{0.05}$ is not suitable for thermoelectric refigulator application because it obtained small surface temperature decreased which affect from high resistance of

thermoelectric devices. The surface temperature can be defined by Eq. 4.4 (Cai, Y., Wangd, Y., Liud, D., and Zhao, F-Y., 2018, pp. 238-255).

$$T_j = \frac{(K-SI)\left(I^2R+\frac{1}{2}SI^3R\right)\left(\frac{1}{2C}R_{ejh}\right)+KT_{in}+\frac{1}{2}I^2R}{+Q_c\left\{1+(K-SI)\left(\frac{1}{2C}+R_{ejh}\right)+R_{ejc}[K+SI-\left(\frac{1}{2C}+R_{ejh}\right)S^2I^2\right\}} \qquad (4.4)$$

where, K is thermal conductance (W K^{-1}), R_{ejh} is thermal resistance in hot side, R_{ejc} is thermal resistance in cold side, C is fluid specific heat (W K^{-1}) and R is thermal resistance (Ω).

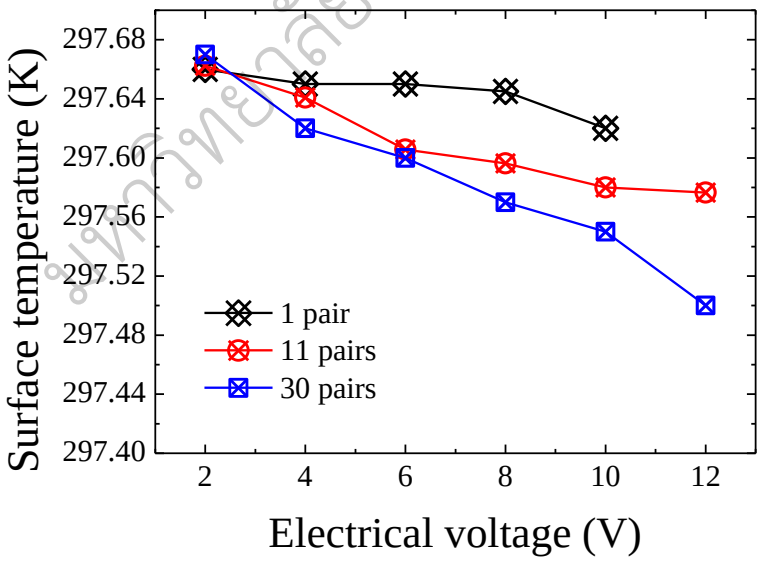

Figure 37 The electrical current dependence on different temperature of thermoelectric devices